Journal of Biomaterials and Nanobiotechnology, 2025, 16(1), 1-20
https://www.scirp.org/journal/jbnb
ISSN Online: 2158-7043
ISSN Print: 2158-7027

Keratinocyte Biocompatibility of Biogenic Iron Nanoparticles

Eliana Daniela Lopez Venditti[1,2], Pamela Soledad Bustos[3], María Natalia Calienni[4,5,6,7], Jorge Montanari[4,5,6], Paulina Laura Paez[3,8], Patricia Angélica Barril[9], María Gabriela Paraje[10,11], Natalia Guiñazú[1,2*]

[1]Centro de Investigaciones en Toxicología Ambiental y Agrobiotecnología del Comahue (CITAAC), Consejo Nacional de Investigaciones Científicas y Técnicas (CONICET), Neuquén, Argentina
[2]Departamento de Ciencias del Ambiente y la Salud, Facultad de Ciencias del Ambiente y la Salud, Universidad Nacional del Comahue, Neuquén, Argentina
[3]Departamento de Ciencias Farmacéuticas, Facultad de Ciencias Químicas, Universidad Nacional de Córdoba, Haya de la Torre y Medina Allende, Córdoba, Argentina
[4]Laboratorio de Bio-Nanotecnología, Departamento de Ciencia y Tecnología, Universidad Nacional de Quilmes, Buenos Aires, Argentina
[5]Grupo de Biología Estructural y Biotecnología (GBEyB), IMBICE (CONICET CCT-La Plata), Buenos Aires, Argentina
[6]Laboratorio de Nanosistemas de Aplicación Biotecnológica (LANSAB), Universidad Nacional de Hurlingham, Buenos Aires, Argentina
[7]Comisión de Investigaciones Científicas de la Provincia de Buenos Aires (CIC), Buenos Aires, Argentina
[8]Unidad de Investigación y Desarrollo en Tecnología Farmacéutica (UNITEFA), Consejo Nacional de Investigaciones Científicas y Técnicas (CONICET), Haya de la Torre y Medina Allende, Córdoba, Argentina
[9]Centro de Investigación y Asistencia Técnica a la Industria (CIATI), Consejo Nacional de Investigaciones Científicas y Técnicas (CONICET), Neuquén, Argentina
[10]Instituto Multidisciplinario de Biología Vegetal (IMBIV), Consejo Nacional de Investigaciones Científicas y Técnicas (CONICET), Córdoba, Argentina
[11]Cátedra de Microbiología, Facultad de Ciencias Exactas, Físicas y Naturales, Universidad Nacional de Córdoba, Córdoba, Argentina
Email: *natanien@hotmail.com, *natalia.guinazu@facias.uncoma.edu.ar

How to cite this paper: Lopez Venditti, E.D., Bustos, P.S., Calienni, M.N., Montanari, J., Paez, P.L., Barril, P.A., Paraje, M.G. and Guiñazú, N. (2025) Keratinocyte Biocompatibility of Biogenic Iron Nanoparticles. *Journal of Biomaterials and Nanobiotechnology*, **16**, 1-20.
https://doi.org/10.4236/jbnb.2025.161001

Received: January 2, 2025
Accepted: January 27, 2025
Published: January 30, 2025

Abstract

Iron nanoparticles (FeNPs) are promising candidates for medical purposes, including topical dermatological applications and skin absorption. This research investigated whether biologically synthesized FeNPs display potential toxic effects in human keratinocytes *in vitro*. Cell cultures were performed with the HaCaT keratinocyte cell line, which was exposed to FeNPs (0 - 214 µg/mL) for 4 and 24 h. Cell viability, reactive oxygen species production, cellular antioxidant components, and wound healing assays were analyzed. FeNPs did not alter the morphology of HaCaT cells, although low cellular cytotoxicity at the highest concentration was observed. The 214 µg/mL condition also

altered cell migration as well as increased reactive oxygen species production. The obtained results have shown that biosynthetic FeNPs display low keratinocyte toxicity and could be explored as promising candidates to be used in local treatments as conjugates for drug delivery systems.

Keywords

Iron Nanoparticles, *E. coli*, Biosynthesis, Keratinocytes, Toxicology

1. Introduction

Metal nanomaterials have been investigated for various applications, including catalytic reactions, medical imaging, biosensors, drug delivery, and biomedical therapy due to their unique physical and chemical properties [1] [2]. In particular, iron oxide nanoparticles (NPs), have gained attention to be promising candidates due to their low toxicity and facile functionalization [3]. Iron and iron oxide NPs are the preferred metal NPs in biomedicine, including anticancer and antiviral therapy, magnetic hyperthermia, resonance imaging, and drug delivery, among others [4]. The Food and Drug Administration (FDA) approved Fe_3O_4/Fe_2O_3 NPs in clinical applications primarily because of their high versatility in surface modification and stability [5].

The synthesis of NPs with biological techniques has several advantages compared to chemical and physical methods, such as being safe to handle, less contaminating, and relatively inexpensive [6]. Metal NPs biosynthesis can be achieved with biological products, plant extracts, and microorganisms such as fungi, algae, and bacteria [6]-[8]. Microorganism-based NPs synthesis has gained popularity because it is easy to perform as it occurs under ambient conditions, produces fewer toxic byproducts, utilizes abundant and renewable metal precursors, and is easily scalable [6]. It has been shown that bacteria are good generators of metallic NPs, either by extracellular or intracellular synthesis [9]. It has been reported that microorganisms such as *Pseudomonas aeruginosa* [10], *Bacillus subtilis* [11], *Bacillus cereus* [12] and *E. coli* have [10] a good capacity to produce iron NPs.

Although metal NPs, in particular iron and iron oxide NPs, hold tremendous potential benefits, there is a significant lack of knowledge concerning their health effects in short- and long-term exposure scenarios [13]. Due to their larger surface area, smaller size, and enhanced chemical reactivity, NPs exhibit potentially higher toxicity than larger particles of the same substance [14]. Dermal exposure is a potential route of exposure to iron and iron oxide NPs because of their manufacturing and innovative use in wound healing [15]. FeNPs possess promising uses in topical treatments [16], however studies assessing skin toxicity are scarce and mainly focused on assessing the biocompatibility of FeNPs obtained by chemical synthesis [17] [18]. Although biogenic NPs show differences in biocompatibility and cell toxicity compared to their chemical counterparts [19] [20], the Biocom-

patibility of biogenic FeNPs has been studied to a lesser extent [21]. Moreover, to our knowledge, the skin biocompatibility of biogenic FeNPs derived from *E. coli* has not been evaluated. Keratinocytes are the major constituent of the epidermis, and the human HaCaT cell line is a valuable model to investigate the toxic effects of NPs on the skin [22] [23].

This work studied the biocompatibility of FeNPs derived from *E. coli* [10], on a human keratinocyte cell model. Possible alterations in cell viability, redox modulation including oxidative and nitrosative stress and antioxidant defenses, were analyzed in HaCaT cells. Taking into account the importance of keratinocytes in the wound-healing process, cell migration was also studied. Our results demonstrate, for the first time, that *E. coli* biogenic FeNPs exhibit a good keratinocyte biocompatibility.

2. Materials and Methods

2.1. HaCaT Cell Culture

The immortalized human keratinocyte cell line HaCaT was grown in RPMI 1640 medium (Sigma Aldrich. St. Louis, MO, USA) supplemented with antibiotic antimycotic solution 1X (Sigma Aldrich. St. Louis, MO, USA) and 10% fetal bovine serum (FBS) (NATOCOR. Córdoba, Argentina). 2×10^6 cells were cultured (37˚C in a 5% CO_2) in a 100 mm Petri dish, until achieving an 80% - 90% confluence. For the following assays FeNPs were used at a concentration range of 26.8 to 214 µg/mL. The concentration range was selected considering previous reports [24] [25] and studies performed in our laboratory [26]. Different conditions were assayed as controls. cells were incubated with RPMI as the basal condition (control) or the metal precursor salt $FeSO_4$. H_2O_2 was used as a positive control for cell viability and ROS assays [27] (data not shown). Conditions were assayed as triplicates and the assays were repeated at least 3 times.

2.2. Cell Viability

The cell viability was assessed using the 3-(4,5-dimethylthiazol-2-yl)-2,5-diphenyl tetrazolium bromide (MTT) assay, neutral red (NR) and crystal violet (CV) [28]. Cells (3×10^4 cells/100 µL) were plated in 96-well plates and then treated with FeNPs (range 214 - 26.8 µg/mL) for 4 and 24 h. Cells were also incubated with medium alone (control) or $FeSO_4$. For the MTT assay, cells were incubated with MTT (0.5 mg/mL) (Sigma Aldrich. St. Louis, MO, USA) in sterile PBS 1X for 1 h at 37˚C. This solution was removed, and the precipitated dye was dissolved in dimethyl sulfoxide (DMSO) (BioPack. Buenos Aires, Argentina) with gentle shaking for 30 min. On the other hand, for the NR test, cells were incubated with NR (50 µg/mL) (BioPack. Buenos Aires, Argentina) in RPMI 1640 medium without phenol red (Sigma Aldrich. St. Louis, MO, USA) for 1 h at 37˚C. This solution was removed and the fixative solution (formaldehyde 1%, calcium carbonate 1%) was added after 2 min and washed once with saline solution (NaCl 0.9%). Finally, the developer solution (ethanol 50%, glacial acetic acid 1%) was added. Lastly, for CV

assay, cells were incubated with CV solution (0.1%, methanol 20%) (BioPack. Buenos Aires, Argentina) for 15 min in a wet chamber. The solution was removed, and the microplate was washed once with distilled water. Finally, acetic acid 30% was added. For MTT, CV, and NR absorbance was recorded at 550 nm (THERMOMAX microplate reader), and the results were expressed as a percentage of control cells maintained with the medium alone.

2.3. Wound Healing Assay

The migratory capacity of HaCaT keratinocytes was evaluated by the wound healing assay according to Grada *et al.* [29]. Briefly, cells were cultured in 96-well plates until 80% - 90% confluence. Then, the cell monolayer was scratched with a small pipette tip (10 µL) to make the wound. Wounds were gently washed with sterile 1X PBS and treated with the previously mentioned conditions. Treatments were prepared in culture medium supplemented with 1% FBS, to minimize cell proliferation. At least 2 wounds were made per treatment and data were obtained from at least three biological replicates. The images were captured after 0, 4 and 24 h treatment. The wound area was measured using the ImageJ program (https://imagej.nih.gov/ij/). Results are expressed as the percentage reduction of wound closure area.

2.4. Reactive Species Analysis

After cellular treatments superoxide anion radical ($O_2^{\bullet-}$) production was evaluated with the nitroblue tetrazolium (NBT) assay [26]. After removing the supernatants, NBT-phorbol 12-myristate 13-acetate (PMA) solution (0.01% - 0.125 µM) (Sigma Aldrich. St. Louis, MO, USA) was added. The plate was incubated at 37˚C for 45 min. Then the solution KOH (2 N) and DMSO was used to solubilize the formazan crystals. Plate absorbance was measured at 630 nm (THERMOMAX microplate reader). The results were expressed as percentages of $O_2^{\bullet-}$ production concerning control cells maintained in the control condition.

Reactive nitrogen species (RNS) production was determined with the Griess reagent (Sigma Aldrich. St. Louis, MO, USA). After treatments culture supernatant (100 µL) was obtained and mixed with the Griess reagent [26]. After 30 min. incubation plate absorbance was measured at 540 nm (THERMOMAX microplate reader). Nitrite concentration was calculated using a sodium nitrite standard curve.

Intracellular ROS were determined with dichloro-dihydro-fluorescein diacetate ($DCFH_2$-DA), as described previously [26]. After treatments, HaCaT cells were incubated with $DCFH_2$-DA (25 µM) (Sigma Aldrich. St. Louis, MO, USA) in the dark for 30 min. at 37˚C. Then, fluorescence was measured (Hitachi H700) and ROS were expressed as relative fluorescence units (RFU).

2.5. Antioxidant Enzyme Activities and GSH Content

Superoxide dismutase (SOD) activity was determined in cultured cells, as described previously [26]. After treatments, cells were incubated with the reaction mixture

containing NBT 75 μM (Sigma Aldrich. St. Louis, MO, USA) in DMSO-PBS 1X, methionine 13 mM (Sigma Aldrich. St. Louis, MO, USA), ethylenediaminetetraacetic acid (EDTA) 100 nM (Sigma Aldrich. St. Louis, MO, USA), and riboflavin 2 μM (Sigma Aldrich. St. Louis, MO, USA) in PBS 1X; for 15 min at 20 W fluorescent light exposure. The absorbance was determined at 560 nm (THERMOMAX microplate reader). A unit of SOD was defined as the quantity of enzyme required to produce a 50% inhibition of NBT reduction.

Catalase (CAT) activity was determined by monitoring the continuous decrease of hydrogen peroxide (H_2O_2) [26]. Cell homogenates were obtained and incubated with sodium-potassium phosphate buffer (50 mM, pH 7.0) and H_2O_2 (81.5 mM). The absorbance was immediately recorded at 240 nm at 37˚C for 60 seg (SHIMADZU UV 1603 spectrophotometer). A unit of CAT was defined as the quantity of enzyme required to consume 1 μmol of H_2O_2 per minute. The extinction coefficient used was $\varepsilon = 40\ M^{-1} \times cm^{-1}$.

Glutathione S-transferase (GST) activity was determined as described previously [26]. cell homogenates were obtained and incubated with sodium phosphate buffer (0.1 M, pH 6.5) with 1-chloro-2,4-dinitrobenzene (CDNB, 50 mM) (Sigma Aldrich. St. Louis, MO, USA) and GSH (50 mM) (Sigma Aldrich. St. Louis, MO, USA). The absorbance was recorded at 340 nm (SHIMADZU UV 1603 spectrophotometer). A unit of GST was defined as the quantity of enzyme required to produce CDNB conjugate (nmol/min). The extinction coefficient used was $\varepsilon = 9.6\ mM^{-1} \times cm^{-1}$.

Glutathione (GSH) content was determined by Ellman's colorimetric assay. Cell homogenates were obtained and incubated with trichloroacetic acid (10%), then centrifuged at 10,000 × g, 4˚C for 10 min. The sample was mixed with Ellman's reagent containing 5,5'-dithiobis-2-nitrobenzoic acid (DTNB) 1.5 mM (Sigma Aldrich. St. Louis, MO, USA) in potassium phosphate buffer 0.25 M, and measured at 412 nm (SHIMADZU UV 1603 spectrophotometer). For GSH quantification calibration curves were carried out with GSH (0 - 16 nmol).

Protein content was quantified by the Bradford method using bovine serum albumin (BSA) as standard.

2.6. Statistical Analysis

Statistical analysis was performed using the GraphPad Prism 8 program (GraphPad Software, CA, USA), one-way analysis of variance (ANOVA), and Dunnet tests were applied for post-hoc analysis. All values are expressed as mean ± SEM. A value of $p < 0.05$ was considered to be statistically significant.

3. Results

3.1. Effect of FeNPs in Keratinocytes Cell Viability

Possible interactions between FeNPs and HaCaT keratinocytes were analyzed, and cell viability was determined by different assays. The MTT reduction assay involves the conversion of the water-soluble yellow dye to an insoluble purple formazan by the action of mitochondrial reductase [30]. The CV assay binds to proteins

and DNA, thus detecting the adherent cell [31]. The NR assay (NR) is based on the ability of viable cells to incorporate and bind the supravital dye NR [32].

Figure 1(a) and Figure 1(b) shows the MTT results after 4 and 24 h treatments. FeNPs significantly reduced cell viability compared to the control condition (complete medium). After 4 h culture 86.39% and 78.81% of viable cells were determined at 107 and 214 μg/mL, respectively. After 24 h culture of 214 μg/mL, significantly induced cell death. Similarly, cell adherence was altered by the highest FeNPs concentrations assayed after 24 h incubation (Figure 1(c) and Figure 1(d)).

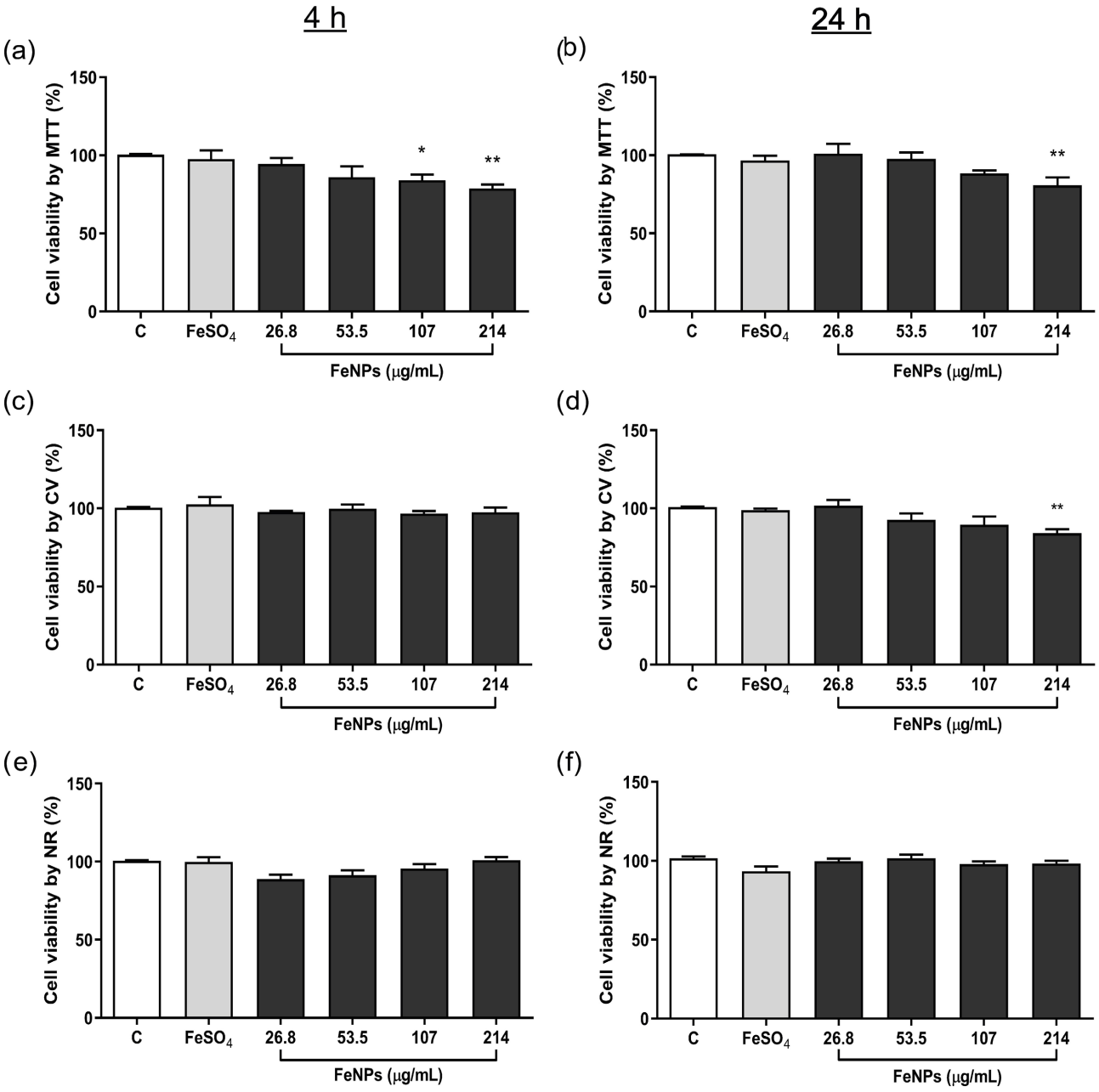

Figure 1. Viability of HaCaT keratinocytes after FeNPs treatment for 4 and 24 h. (a) (b) Cell viability was determined by MTT, (c) (d) crystal violet (CV), and (e) (f) neutral red (NR) assays. Cell viability is expressed as percentages (mean ± SEM). *$p < 0.05$, **$p < 0.01$, statistical difference compared to control cells.

The NR assay indicated non-significant changes in all the conditions assayed (Figure 1(e) and Figure 1(f)).

3.2. Effect of FeNPs in Keratinocytes Cell Morphology and Migration

As observed in Figure 2, all the conditions assayed did not affect the cell morphology. The scratch-wound assay was carried out to determine the FeNPs effect on the

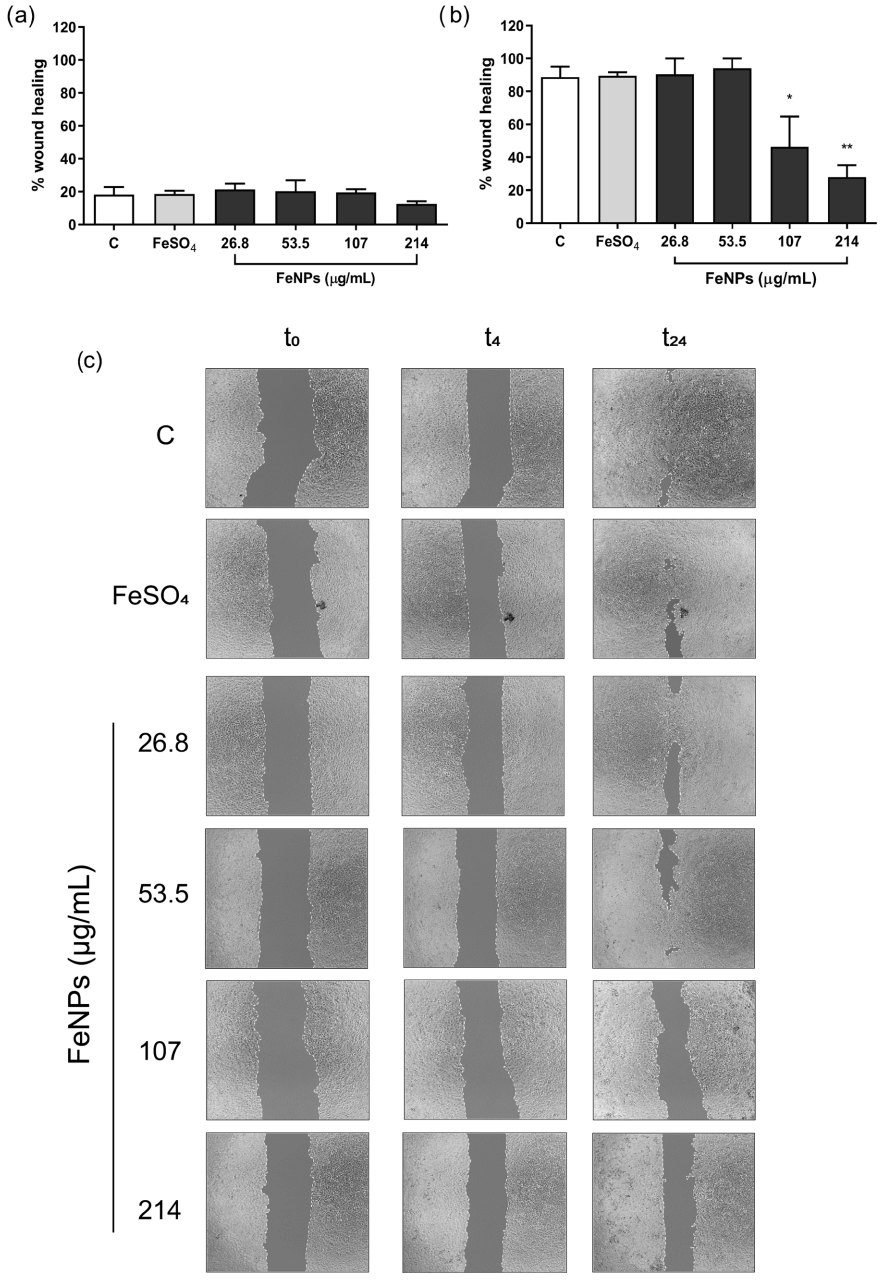

Figure 2. Wound healing assay of HaCaT cells treated with FeNPs. (a) Percentage of wound healing at 4 h, mean ± SEM; (b) Percentage of wound healing at 24 h, mean ± SEM. *$p < 0.05$, **$p < 0.01$, statistical differences compared to control cells. Bar graphs show the mean ± SEM of three independent biological replicates; (c) Representative Images of the wound healing process after 4 and 24 h exposure to FeNPs.

migration of HaCaT cells into cell-free scratch-wounded areas after 4 and 24 h treatments. The percentage of wound closure after 4 h, showed non-significant changes among treatments. However, after 24 h incubation, the higher FeNPs concentrations (107 and 214 μg/mL) significantly altered cell migration and diminished the wound closure.

3.3. Effect of FeNPs on ROS and RNS Levels

The incubation with 214 μg/mL FeNPs induced a significant increase in $O_2^{\bullet-}$ production after 4 h (130.4%) and 24 h (118%) with respect to control cells (Figure 3(a) and Figure 3(b)). A higher range of ROS was also determined with the $DCFH_2$-DA reagent. FeNPs 214 μg/mL treatment, for 4 h and 24 h, significantly increased 2.3 times the ROS production in comparison to the control condition (Figure 3(c) and Figure 3(d)). No significant changes in RNS levels were observed in HaCaT cells after exposure for 4 and 24 h, for all treatments (data not shown).

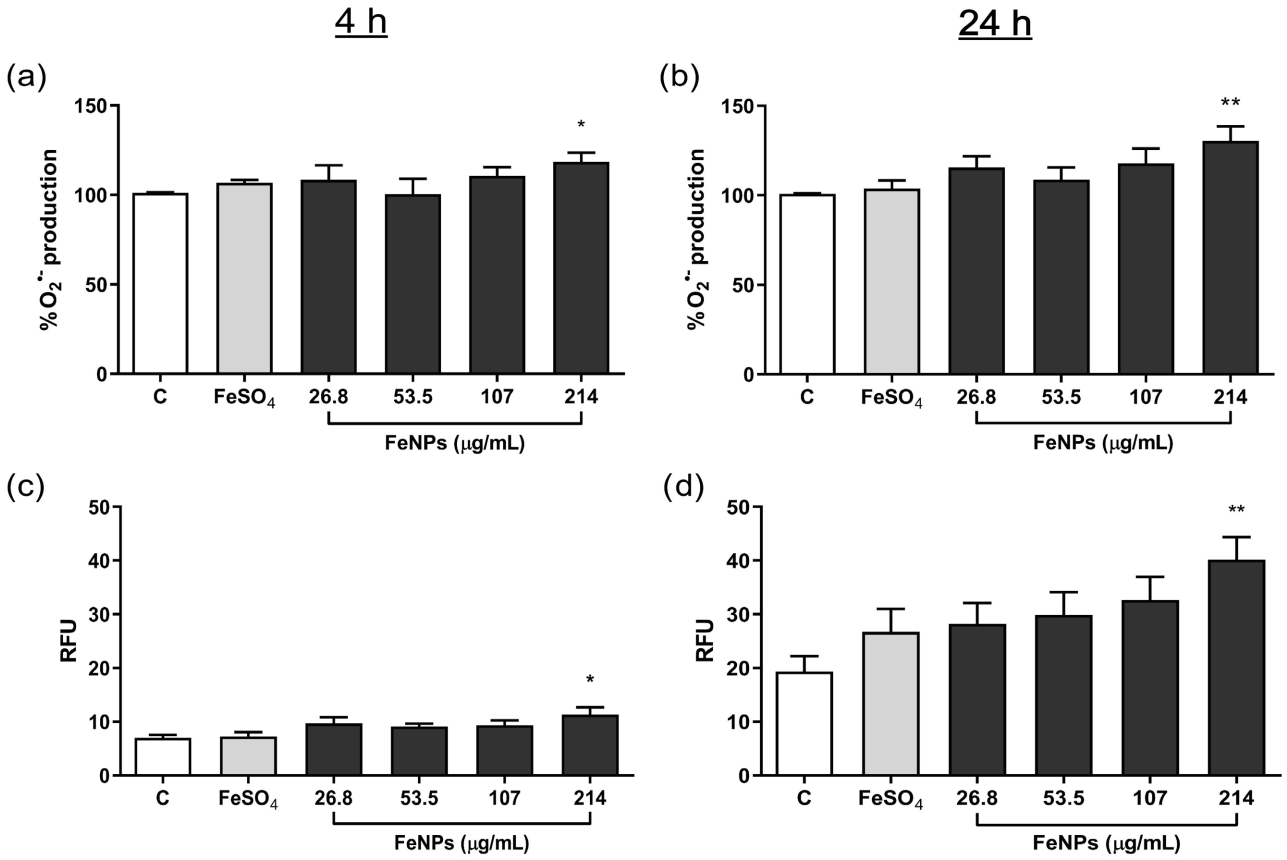

Figure 3. Reactive oxygen species (ROS) production after 4 and 24 h exposure to FeNPs. (a) (b) Levels of superoxide anion after 4 and 24 h exposure to FeNPs. NBT reduction is expressed as percentages (mean ± SEM). (c) (d) Levels of intracellular ROS by $DCFH_2$-DA after 4 and 24 h exposure to FeNPs. Relative fluorescence units (RFU) are expressed as the mean ± SEM. *$p < 0.05$, **$p < 0.01$, statistical differences compared to control.

3.4. Effect of FeNPs in Keratinocytes Antioxidant Cellular Defenses

Possible alterations in redox homeostasis were evaluated by the determination of

enzymes important for antioxidant cellular defenses such as SOD, CAT, and GST. The cellular content of the GSH was also determined.

FeNPs at 53.5, 107, and 214 μg/mL significantly modify SOD activity after 4 h exposure. In contrast, after 24 h treatments showed non-significant changes in SOD activity (**Figure 4(a)** and **Figure 4(b)**). CAT and GST activity and GSH levels showed non-significant changes among treatments after 4 and 24 h incubations (**Figures 4(c)-(h)**).

4. Discussion

Microorganisms can produce inorganic materials at the nanoscale, either intra- or extracellularly. These organisms can reduce and accumulate metal ions when exposed to metal ion solutions, as detoxification and homeostasis mechanisms [33]. Microorganisms as *Ralstonia pickettii* sp. [34], *Pseudomonas aeruginosa* [10], *Bacillus subtilis* [35] and *Bacillus cereus* [12] were used for either for intracellular or extracellular synthesis of FeNPs. *E. coli* is a bacterium able to produce different nanomaterials such as quantum dots and NPs [36]-[38]. Previously, Crespo *et al.* [10] optimized the environmentally friendly process of biosynthesis of iron NPs intra- and extracellular employing prokaryotic microorganisms that showed anticoagulant activity by the activation of the extrinsic pathway [10]. The results presented here demonstrated the reproducibility of FeNPs green synthesis using *E. coli*. Similar to Crespo *et al.*, the FeNPs obtained here had a size of 20.7 ± 6.1 nm, a negative Z potential of −10.9 mV, and a spherical shape [10]. On the other hand, characterization by FT-IR spectroscopy showed the presence of absorption bands characteristic of proteins, amides and polysaccharides. These were later related to the presence of proteins observed in the silver-stained gel, indicating that FeNPs may be stabilized by amino acid and protein coating. The presence of iron was also confirmed by the plasmon appearance and the Fe-O signal in the FT-IR analysis. It has been postulated that one of the main challenges when using biogenic precursors is to achieve the reproducibility of the synthesis method [39], which is essential to reproduce the specific characteristics and properties of the synthesized nanoparticles. Also, the scaling capabilities of the NPs bioprocess strongly depend on the biosynthesis reproducibility.

Different types of FeNPs can be synthesized using the physical, chemical, and biological methods [40], resulting in FeNPs with different characteristics and properties. Thus, metal salt precursor as well as the synthesis mode are crucial to define the FeNPs properties and biocompatibility. Studies have demonstrated better biocompatibility of biogenic green FeNPs compared to chemical FeNPs [19] [20]. Most of the published reports have evaluated the biocompatibility of iron oxide NPs in different cell types, including macrophages [41], endothelial [42], and fibroblasts [43]. Although potential uses of FeNPs include topical dermal applications [44]-[46], and transdermal drug delivery carriers [47], investigations of possible toxic effects on keratinocytes and epidermal cells are limited. Moreover, it has been postulated that one of the primary pathways for the entry of NPs

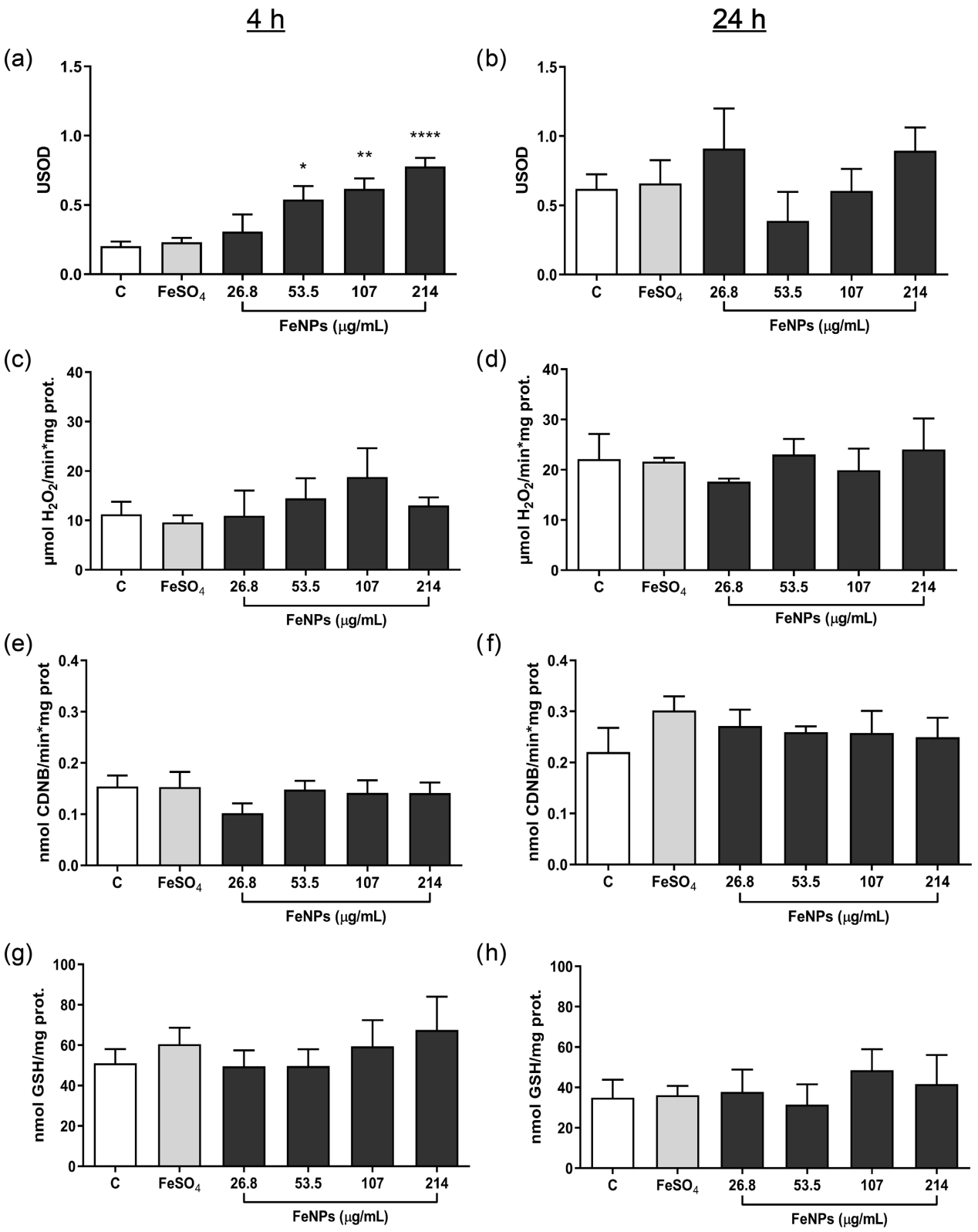

Figure 4. Antioxidant defenses of HaCaT cells treated with FeNPs for 4 and 24 h. (a) (b) Superoxide dismutase activity is expressed as units of SOD (USOD, mean ± SEM). (c) (d) Catalase activity is expressed as µmol of consumed H_2O_2 per min per mg of protein (mean ± SEM). (e) (f) Glutathione-S-transferase activity is expressed as nmol of conjugated CDNB per min per mg of protein (mean ± SEM). (g) (h) Glutathione content is expressed as nmol of GSH per mg of protein (mean ± SEM). *$p < 0.05$, **$p < 0.01$, ****$p < 0.0001$.

into the body involves absorption through the skin, comprehensive investigation into the cutaneous toxicity of NPs remains scarce [48]. Toxicity studies have been focused on investigating the toxic effect of FeNPs from either chemical or plant biological synthesis [21], neglecting the toxicity research of biogenic microbial FeNPs.

In this work, microbial biosynthesized FeNPs did not alter the HaCaT cell morphology, although cells developed minor cytotoxicity at the highest concentration assayed. Thus, an important percentage of cells remained viable after 4 h and 24 h incubation, a 78.81% and an 80.72%, respectively. Similarly, FeNPs obtained from biological synthesis using *Artemisia absinthium L.* [21] demonstrated a low toxicity, as the HaCaT viable population did not decrease beyond 80%. Moreover, FeNPs from solution combustion synthesis [47], did not alter cell viability after 24 h exposure to 25 μg/mL concentration. Amin *et al.* (2014) have investigated the keratinocyte toxicity of photochemically obtained Fe_3O_4 NPs and reported no cytotoxicity within the tested concentrations (up to 500 μg/mL) [49]. In our work, the low cytotoxicity observed with the MTT method was confirmed with two additional methods. CV showed a minor decrease in cell viability with the highest concentration assayed after 24 h exposure, whereas NR uptake showed non-significant changes. Differences were observed between the MTT, CV, and NR assays, likely due to their distinct mechanisms: the MTT assay measures mitochondrial succinate dehydrogenase activity, the CV assay detects adherent cells [31], and the NR assay assesses the ability of cells to maintain pH gradients through ATP production [32]. Thus, FeNPs interact with HaCaT cells at high concentrations, mainly altering mitochondria activity at the highest concentration. Nevertheless, one of the drawbacks of using cell lines to assay toxicity is the inability to fully reproduce the complexity of the skin and the cellular heterogeneity under basal or inflammatory conditions. This highlights the need for further studies on the interactions of FeNPs with other cells relevant to skin integrity, such as fibroblasts, as well as in *in vivo* models under acute and chronic exposure scenarios.

The condition that decreased cell viability also altered cell migration as well as increased ROS. Although antioxidant defenses were induced at short incubation times, the increase in SOD activity was not sufficient to mitigate oxidative stress at the highest concentration tested. The excess of ROS observed at the highest concentrations of FeNPs reveals the insufficiency of the endogenous antioxidant system to counteract ROS. It has been postulated that ROS could trigger the oxidation of the main macromolecules such as lipids, proteins and DNA, generating cellular alterations with the consequent decrease in cell viability [26]. Different mechanisms are proposed for the cytotoxic effect of FeNPs in diverse cell types, such as release of iron ions, the ROS production and genotoxicity [50] [51]. These effects can be explained by the large amount of Fe^{2+}/Fe^{3+} ions exposed on the large surface of iron oxide nanoparticles [51]. It has been reported that upon entering the cell, NPs could release ferric ions which generate H_2O_2 radicals, hydroxyl radicals, and ferrous ions by the Fenton reaction [52]. Excess of iron ions will cause

overproduction of ROS, which can damage cellular compartments and oxidize lipids, proteins, and DNA. It has been shown that the cytotoxicity generated by FeNPs in human fibroblasts would be related to DNA oxidation [51]. Furthermore, it has been reported that prolonged exposure to iron oxide NPs could induce the loss of cellular GSH from various proteins [53]. However, the FeNPs reported here did not generate changes in glutathione content in HaCaT keratinocytes. Further studies evaluating the possible oxidation of protein, lipids and DNA in keratinocytes will be necessary to elucidate the mechanism of toxicity manifested by biogenic FeNPs at high concentration.

5. Conclusion

FeNPs "green synthesis" has found wide applications in different fields of biomedicine. Here we have shown that FeNPs "green synthesis" by *E. coli* is a reproducible bioprocess in which the biogenic FeNPs display low toxicity and could be explored as promising candidates to be used as conjugates for drug delivery systems. Moreover, the topical dermal use and the skin absorption pathway represent a promising FeNPs treatment targets and administration route.

Acknowledgements

This work is part of the Ph. D. thesis of the first author who thanks the CONICET for her doctoral fellowship.

Conflicts of Interest

The authors declare no conflicts of interest regarding the publication of this paper.

References

[1] Choi, Y. and Lee, S.Y. (2020) Biosynthesis of Inorganic Nanomaterials Using Microbial Cells and Bacteriophages. *Nature Reviews Chemistry*, **4**, 638-656. https://doi.org/10.1038/s41570-020-00221-w

[2] Andleeb, A., Andleeb, A., Asghar, S., Zaman, G., Tariq, M., Mehmood, A., *et al.* (2021) A Systematic Review of Biosynthesized Metallic Nanoparticles as a Promising Anti-Cancer-Strategy. *Cancers*, **13**, Article 2818. https://doi.org/10.3390/cancers13112818

[3] Malhotra, N., Lee, J., Liman, R.A.D., Ruallo, J.M.S., Villaflores, O.B., Ger, T., *et al.* (2020) Potential Toxicity of Iron Oxide Magnetic Nanoparticles: A Review. *Molecules*, **25**, Article 3159. https://doi.org/10.3390/molecules25143159

[4] Cotin, G., Piant, S., Mertz, D., Felder-Flesch, D. and Begin-Colin, S. (2018) Iron Oxide Nanoparticles for Biomedical Applications: Synthesis, Functionalization, and Application. In: Mahmoudi, M. and Laurent, S., Eds., *Iron Oxide Nanoparticles for Biomedical Applications*, Elsevier, 43-88. https://doi.org/10.1016/b978-0-08-101925-2.00002-4

[5] Ribeiro, A.I., Dias, A.M. and Zille, A. (2022) Synergistic Effects between Metal Nanoparticles and Commercial Antimicrobial Agents: A Review. *ACS Applied Nano Materials*, **5**, 3030-3064. https://doi.org/10.1021/acsanm.1c03891

[6] Park, T.J., Lee, K.G. and Lee, S.Y. (2015) Advances in Microbial Biosynthesis of Metal

Nanoparticles. *Applied Microbiology and Biotechnology*, **100**, 521-534. https://doi.org/10.1007/s00253-015-6904-7

[7] Zafar, N., Madni, A., Khalid, A., Khan, T., Kousar, R., Naz, S.S., *et al.* (2020) Pharmaceutical and Biomedical Applications of Green Synthesized Metal and Metal Oxide Nanoparticles. *Current Pharmaceutical Design*, **26**, 5844-5865. https://doi.org/10.2174/1381612826666201126144805

[8] Franceschinis, G., Beverina, M., Corleto, M., Sosa, A.M., Lillo, C., Arias Casará, L., *et al.* (2023) Green-Synthesized Silver Nanoparticles Using Aloe Maculata Extract as Antibacterial Agent for Potential Topical Application. *OpenNano*, **12**, Article ID: 100148. https://doi.org/10.1016/j.onano.2023.100148

[9] Tsekhmistrenko, S.I., Bityutskyy, V.S., Tsekhmistrenko, O.S., Horalskyi, L.P., Tymoshok, N.O. and Spivak, M.Y. (2020) Bacterial Synthesis of Nanoparticles: A Green Approach. *Biosystems Diversity*, **28**, 9-17. https://doi.org/10.15421/012002

[10] Crespo, K.A., Baronetti, J.L., Quinteros, M.A., Páez, P.L. and Paraje, M.G. (2016) Intra- and Extracellular Biosynthesis and Characterization of Iron Nanoparticles from Prokaryotic Microorganisms with Anticoagulant Activity. *Pharmaceutical Research*, **34**, 591-598. https://doi.org/10.1007/s11095-016-2084-0

[11] Sundaram, P.A., Augustine, R. and Kannan, M. (2012) Extracellular Biosynthesis of Iron Oxide Nanoparticles by *Bacillus subtilis* Strains Isolated from Rhizosphere Soil. *Biotechnology and Bioprocess Engineering*, **17**, 835-840. https://doi.org/10.1007/s12257-011-0582-9

[12] Fatemi, M., Mollania, N., Momeni-Moghaddam, M. and Sadeghifar, F. (2018) Extracellular Biosynthesis of Magnetic Iron Oxide Nanoparticles by Bacillus Cereus Strain HMH1: Characterization and *in Vitro* Cytotoxicity Analysis on MCF-7 and 3T3 Cell Lines. *Journal of Biotechnology*, **270**, 1-11. https://doi.org/10.1016/j.jbiotec.2018.01.021

[13] Sani, A., Cao, C. and Cui, D. (2021) Toxicity of Gold Nanoparticles (AuNPs): A Review. *Biochemistry and Biophysics Reports*, **26**, Article ID: 100991. https://doi.org/10.1016/j.bbrep.2021.100991

[14] Abbasi, R., Shineh, G., Mobaraki, M., Doughty, S. and Tayebi, L. (2023) Structural Parameters of Nanoparticles Affecting Their Toxicity for Biomedical Applications: A Review. *Journal of Nanoparticle Research*, **25**, Article No. 43. https://doi.org/10.1007/s11051-023-05690-w

[15] Thomas, A., Sankaranarayanan, S.A. and Rengan, A.K. (2022) Modified Polyethylene Glycol Encapsulated Iron Oxide Nanoparticles for Accelerated Wound Healing Application. *IEEE Transactions on Nanotechnology*, **21**, 1-5. https://doi.org/10.1109/tnano.2021.3138260

[16] Rao, Y., Chen, W., Liang, X., Huang, Y., Miao, J., Liu, L., *et al.* (2014) Epirubicin-loaded Superparamagnetic Iron-Oxide Nanoparticles for Transdermal Delivery: Cancer Therapy by Circumventing the Skin Barrier. *Small*, **11**, 239-247. https://doi.org/10.1002/smll.201400775

[17] Murray, A.R., Kisin, E., Inman, A., Young, S., Muhammed, M., Burks, T., *et al.* (2012) Oxidative Stress and Dermal Toxicity of Iron Oxide Nanoparticles *in Vitro*. *Cell Biochemistry and Biophysics*, **67**, 461-476. https://doi.org/10.1007/s12013-012-9367-9

[18] Alili, L., Chapiro, S., Marten, G.U., Schmidt, A.M., Zanger, K. and Brenneisen, P. (2015) Effect of Fe_3o_4nanoparticles on Skin Tumor Cells and Dermal Fibroblasts. *BioMed Research International*, **2015**, Article ID: 530957. https://doi.org/10.1155/2015/530957

[19] Dowlath, M.J.H., Musthafa, S.A., Mohamed Khalith, S.B., Varjani, S., Karuppannan, S.K., Ramanujam, G.M., *et al.* (2021) Comparison of Characteristics and Biocompatibility of Green Synthesized Iron Oxide Nanoparticles with Chemical Synthesized Nanoparticles. *Environmental Research*, **201**, Article ID: 111585. https://doi.org/10.1016/j.envres.2021.111585

[20] Iqbal, J., Abbasi, B.A., Batool, R., Khalil, A.T., Hameed, S., Kanwal, S., *et al.* (2019) Biogenic Synthesis of Green and Cost Effective Cobalt Oxide Nanoparticles Using *Geranium wallichianum* Leaves Extract and Evaluation of *in Vitro* Antioxidant, Antimicrobial, Cytotoxic and Enzyme Inhibition Properties. *Materials Research Express*, **6**, Article ID: 115407. https://doi.org/10.1088/2053-1591/ab4f04

[21] Moacă, E., Watz, C.G., Flondor (Ionescu), D., Păcurariu, C., Tudoran, L.B., Ianoş, R., *et al.* (2022) Biosynthesis of Iron Oxide Nanoparticles: Physico-Chemical Characterization and Their *in Vitro* Cytotoxicity on Healthy and Tumorigenic Cell Lines. *Nanomaterials*, **12**, Article 2012. https://doi.org/10.3390/nano12122012

[22] Magogotya, M., Vetten, M., Roux-van der Merwe, M., Badenhorst, J. and Gulumian, M. (2022) *In Vitro* Toxicity and Internalization of Gold Nanoparticles (AuNPs) in Human Epithelial Colorectal Adenocarcinoma (Caco-2) Cells and the Human Skin Keratinocyte (HaCaT) Cells. *Mutation Research/Genetic Toxicology and Environmental Mutagenesis*, **883**, 503556. https://doi.org/10.1016/j.mrgentox.2022.503556

[23] Zanette, C., Pelin, M., Crosera, M., Adami, G., Bovenzi, M., Larese, F.F., *et al.* (2011) Silver Nanoparticles Exert a Long-Lasting Antiproliferative Effect on Human Keratinocyte HaCaT Cell Line. *Toxicology in Vitro*, **25**, 1053-1060. https://doi.org/10.1016/j.tiv.2011.04.005

[24] Perveen, S., Nadeem, R., Rehman, S.u., Afzal, N., Anjum, S., Noreen, S., *et al.* (2022) Green Synthesis of Iron (Fe) Nanoparticles Using *Plumeria obtusa* Extract as a Reducing and Stabilizing Agent: Antimicrobial, Antioxidant and Biocompatibility Studies. *Arabian Journal of Chemistry*, **15**, Article ID: 103764. https://doi.org/10.1016/j.arabjc.2022.103764

[25] Zangeneh, A., Zangeneh, M.M. and Moradi, R. (2019) Ethnomedicinal Plant-Extract-assisted Green Synthesis of Iron Nanoparticles Using *Allium saralicum* Extract, and Their Antioxidant, Cytotoxicity, Antibacterial, Antifungal and Cutaneous Wound-healing Activities. *Applied Organometallic Chemistry*, **34**, e5247. https://doi.org/10.1002/aoc.5247

[26] Bustos, P.S., Quinteros, M.d.l.Á., Gomez, D.S., Ortega, M.G., Páez, P.L. and Guiñazú, N.L. (2021) Silver Bionanoparticles Toxicity in Trophoblast Is Mediated by Nitric Oxide and Glutathione Pathways. *Toxicology*, **454**, Article ID: 152741. https://doi.org/10.1016/j.tox.2021.152741

[27] Zhang, J., Wang, W. and Mao, X. (2020) Chitopentaose Protects HaCaT Cells against H_2O_2-Induced Oxidative Damage through Modulating MAPKs and Nrf2/ARE Signaling Pathways. *Journal of Functional Foods*, **72**, Article ID: 104086. https://doi.org/10.1016/j.jff.2020.104086

[28] Calienni, M.N., Temprana, C.F., Prieto, M.J., Paolino, D., Fresta, M., Tekinay, A.B., *et al.* (2017) Nano-Formulation for Topical Treatment of Precancerous Lesions: Skin Penetration, *in Vitro*, and *in Vivo* Toxicological Evaluation. *Drug Delivery and Translational Research*, **8**, 496-514. https://doi.org/10.1007/s13346-017-0469-1

[29] Grada, A., Otero-Vinas, M., Prieto-Castrillo, F., Obagi, Z. and Falanga, V. (2017) Research Techniques Made Simple: Analysis of Collective Cell Migration Using the Wound Healing Assay. *Journal of Investigative Dermatology*, **137**, e11-e16. https://doi.org/10.1016/j.jid.2016.11.020

[30] Kumar, P., Nagarajan, A. and Uchil, P.D. (2018) Analysis of Cell Viability by the MTT Assay. *Cold Spring Harbor Protocols*, No. 6, 469-471. https://doi.org/10.1101/pdb.prot095505

[31] Feoktistova, M., Geserick, P. and Leverkus, M. (2016) Crystal Violet Assay for Determining Viability of Cultured Cells. *Cold Spring Harbor Protocols*, No. 4, 343-346. https://doi.org/10.1101/pdb.prot087379

[32] Repetto, G., del Peso, A. and Zurita, J.L. (2008) Neutral Red Uptake Assay for the Estimation of Cell Viability/cytotoxicity. *Nature Protocols*, **3**, 1125-1131. https://doi.org/10.1038/nprot.2008.75

[33] Narayanan, K.B. and Sakthivel, N. (2010) Biological Synthesis of Metal Nanoparticles by Microbes. *Advances in Colloid and Interface Science*, **156**, 1-13. https://doi.org/10.1016/j.cis.2010.02.001

[34] Kianpour, S., Ebrahiminezhad, A., Negahdaripour, M., Mohkam, M., Mohammadi, F., Niknezhad, S.V., *et al.* (2018) Characterization of Biogenic Fe (III)-Binding Exopolysaccharide Nanoparticles Produced by *Ralstonia sp. Sk*03. *Biotechnology Progress*, **34**, 1167-1176. https://doi.org/10.1002/btpr.2660

[35] Jubran, A.S., Al-Zamely, O.M. and Al-Ammar, M.H. (2020) A Study of Iron Oxide Nanoparticles Synthesis by Using Bacteria. *International Journal of Pharmaceutical Quality Assurance*, **11**, 88-92. https://doi.org/10.25258/ijpqa.11.1.13

[36] Jiang, X., Fan, X., Xu, W., Zhang, R. and Wu, G. (2019) Biosynthesis of Bimetallic Au-Ag Nanoparticles Using *Escherichia coli* and Its Biomedical Applications. *ACS Biomaterials Science & Engineering*, **6**, 680-689. https://doi.org/10.1021/acsbiomaterials.9b01297

[37] Mi, C., Wang, Y., Zhang, J., Huang, H., Xu, L., Wang, S., *et al.* (2011) Biosynthesis and Characterization of CDs Quantum Dots in Genetically Engineered *Escherichia coli*. *Journal of Biotechnology*, **153**, 125-132. https://doi.org/10.1016/j.jbiotec.2011.03.014

[38] Gurunathan, S., Kalishwaralal, K., Vaidyanathan, R., Venkataraman, D., Pandian, S.R.K., Muniyandi, J., *et al.* (2009) Biosynthesis, Purification and Characterization of Silver Nanoparticles Using *Escherichia coli*. *Colloids and Surfaces B: Biointerfaces*, **74**, 328-335. https://doi.org/10.1016/j.colsurfb.2009.07.048

[39] Murillo-Rábago, E.I., Vilchis-Nestor, A.R., Juarez-Moreno, K., Garcia-Marin, L.E., Quester, K. and Castro-Longoria, E. (2022) Optimized Synthesis of Small and Stable Silver Nanoparticles Using Intracellular and Extracellular Components of Fungi: An Alternative for Bacterial Inhibition. *Antibiotics*, **11**, Article 800. https://doi.org/10.3390/antibiotics11060800

[40] Nkosi, N.C., Basson, A.K., Ntombela, Z.G., Dlamini, N.G. and Pullabhotla, R.V.S.R. (2025) Green Synthesis and Characterization of Iron Nanoparticles Synthesized from Bioflocculant for Wastewater Treatment: A Review. *Biotechnology Notes*, **6**, 10-31. https://doi.org/10.1016/j.biotno.2024.12.001

[41] Siglienti, I., Bendszus, M., Kleinschnitz, C. and Stoll, G. (2006) Cytokine Profile of Iron-Laden Macrophages: Implications for Cellular Magnetic Resonance Imaging. *Journal of Neuroimmunology*, **173**, 166-173. https://doi.org/10.1016/j.jneuroim.2005.11.011

[42] Moore, A., Marecos, E., Bogdanov, A. and Weissleder, R. (2000) Tumoral Distribution of Long-Circulating Dextran-Coated Iron Oxide Nanoparticles in a Rodent Model. *Radiology*, **214**, 568-574. https://doi.org/10.1148/radiology.214.2.r00fe19568

[43] Berry, C.C., Wells, S., Charles, S., Aitchison, G. and Curtis, A.S.G. (2004) Cell

Response to Dextran-Derivatised Iron Oxide Nanoparticles Post Internalisation. *Biomaterials*, **25**, 5405-5413. https://doi.org/10.1016/j.biomaterials.2003.12.046

[44] Sathiyaseelan, A., Saravanakumar, K., Mariadoss, A.V.A. and Wang, M. (2021) Antimicrobial and Wound Healing Properties of FeO Fabricated Chitosan/PVA Nanocomposite Sponge. *Antibiotics*, **10**, Article 524. https://doi.org/10.3390/antibiotics10050524

[45] Zangeneh, M.M., Ghaneialvar, H., Akbaribazm, M., Ghanimatdan, M., Abbasi, N., Goorani, S., *et al.* (2019) Novel Synthesis of *Falcaria vulgaris* Leaf Extract Conjugated Copper Nanoparticles with Potent Cytotoxicity, Antioxidant, Antifungal, Antibacterial, and Cutaneous Wound Healing Activities under *in Vitro* and *in Vivo* Condition. *Journal of Photochemistry and Photobiology B*: *Biology*, **197**, Article ID: 111556. https://doi.org/10.1016/j.jphotobiol.2019.111556

[46] Nahari, M.H., Al Ali, A., Asiri, A., Mahnashi, M.H., Shaikh, I.A., Shettar, A.K., *et al.* (2022) Green Synthesis and Characterization of Iron Nanoparticles Synthesized from Aqueous Leaf Extract of Vitex Leucoxylon and Its Biomedical Applications. *Nanomaterials*, **12**, Article 2404. https://doi.org/10.3390/nano12142404

[47] Coricovac, D., Moacă, E., Pinzaru, I., Cîtu, C., Soica, C., Mihali, C., *et al.* (2017) Biocompatible Colloidal Suspensions Based on Magnetic Iron Oxide Nanoparticles: Synthesis, Characterization and Toxicological Profile. *Frontiers in Pharmacology*, **8**, Article 154. https://doi.org/10.3389/fphar.2017.00154

[48] Nowak-Jary, J. and Machnicka, B. (2024) Comprehensive Analysis of the Potential Toxicity of Magnetic Iron Oxide Nanoparticles for Medical Applications: Cellular Mechanisms and Systemic Effects. *International Journal of Molecular Sciences*, **25**, Article 12013. https://doi.org/10.3390/ijms252212013

[49] Amin, R.M., Abdelmonem, A., Verwanger, T., Elsherbini, E. and Krammer, B. (2014) Cytotoxicity of Magnetic Nanoparticles on Normal and Malignant Human Skin Cells. *Nano LIFE*, **4**, Article ID: 1440002. https://doi.org/10.1142/s1793984414400029

[50] Arias, L.S., Pessan, J.P., Vieira, A.P.M., Lima, T.M.T.d., Delbem, A.C.B. and Monteiro, D.R. (2018) Iron Oxide Nanoparticles for Biomedical Applications: A Perspective on Synthesis, Drugs, Antimicrobial Activity, and Toxicity. *Antibiotics*, **7**, Article 46. https://doi.org/10.3390/antibiotics7020046

[51] Abakumov, M.A., Semkina, A.S., Skorikov, A.S., Vishnevskiy, D.A., Ivanova, A.V., Mironova, E., *et al.* (2018) Toxicity of Iron Oxide Nanoparticles: Size and Coating Effects. *Journal of Biochemical and Molecular Toxicology*, **32**, e22225. https://doi.org/10.1002/jbt.22225

[52] Snezhkina, A.V., Kudryavtseva, A.V., Kardymon, O.L., Savvateeva, M.V., Melnikova, N.V., Krasnov, G.S., *et al.* (2019) ROS Generation and Antioxidant Defense Systems in Normal and Malignant Cells. *Oxidative Medicine and Cellular Longevity*, **2019**, Article ID: 6175804. https://doi.org/10.1155/2019/6175804

[53] Yarjanli, Z., Ghaedi, K., Esmaeili, A., Rahgozar, S. and Zarrabi, A. (2017) Iron Oxide Nanoparticles May Damage to the Neural Tissue through Iron Accumulation, Oxidative Stress, and Protein Aggregation. *BMC Neuroscience*, **18**, Article No. 51. https://doi.org/10.1186/s12868-017-0369-9

Supplementary Material

1. Materials and Methods for Iron NPs Biosynthesis and Characterization

Iron NPs were biosynthesized as previously reported [1]. Briefly, 50 mL of 1 mM $FeSO_4$ (Cicarelli. Santa Fe, Argentina) solution was added to 50 mL *Escherichia coli* ATCC 25922 culture (1×10^9 colony-forming units -CFU/mL) in Luria Bertani (LB) medium (MP BIOMEDICALS, Irvine, CA, USA). After 48 h of constant stirring at 37˚C, the mixture was sonicated at 469W, 47 KHz, for 30 min, and the supernatant was obtained after being centrifuged (3500 rpm) 3 times for 15 min. Finally, supernatant was filtered twice with 0.45 µm and 0.22 µm filters. FeNPs were obtained after centrifuging the supernatant at 20,000 ×g for 20 min. FeNPs were resuspended in milliQ water and then lyophilized (BioBase Lyophilizer Model BK-FD10 Series) at −60˚C/−70˚C and 10 kPa, to determine their concentration.

The NPs bioproduction was regularly checked by the color change of the reaction mixture and by UV-vis spectroscopy. Zeta potential of FeNPs was measured with Zetasizer Nano ZS (Malvern Panalytical). Dynamic light scattering (DLS) (Zetasizer Nano ZS, Malvern Panalytical) and transmission electron microscopy (TEM) (JEM-JEOL 1120 EXII), were performed to determine FeNPs size and shape, respectively.

Fourier-transform infrared spectroscopy (FT-IR) was performed with a spectrometer equipped with a deuterated L-alanine-doped triglycine sulfate detector (DLATGS) in the range from 4000 to 400 cm^{-1} (Shimadzu IRTracer-100). FeNPs samples were prepared in a potassium bromide tablet, containing 300 mg of potassium bromide and 3 mg of FeNPs, and compressed for the tablet formation with a hydraulic press. In addition, to determine the presence of proteins in the FeNPs, SDS-PAGE (12% gel) electrophoresis was performed (Mini-PROTEAN® Tetra Cell 4-gel handcasting system, BioRad). The gels were stained with a silver nitrate solution to reveal the protein bands. FeNPs have a long-term stability of 24 months.

2. Results

2.1. FeNPs Biosynthesis and Characterization

The synthesis of FeNPs, after 48 h *E. coli* culture, was determined spectrophotometrically with the presence of a 294 nm peak, which corresponded to the FeNPs surface plasmon resonance (Supplementary **Figure S1(a)**). In addition, a visual change in color from yellow (control SN) to orange in the culture supernatant incubated with Fe^{2+} ions, was observed (Supplementary **Figure S1(a)**). The morphology and structure of the FeNPs were investigated by TEM (Supplementary **Figure S1(b)**). The TEM image indicated that FeNPs are spherical with an average diameter of 20.7 ± 6.1 nm. The hydrodynamic diameter (Hd) of FeNPs was determined by DLS. NPs have a Hd of 201.7 ± 26.6 nm and a polydispersity index

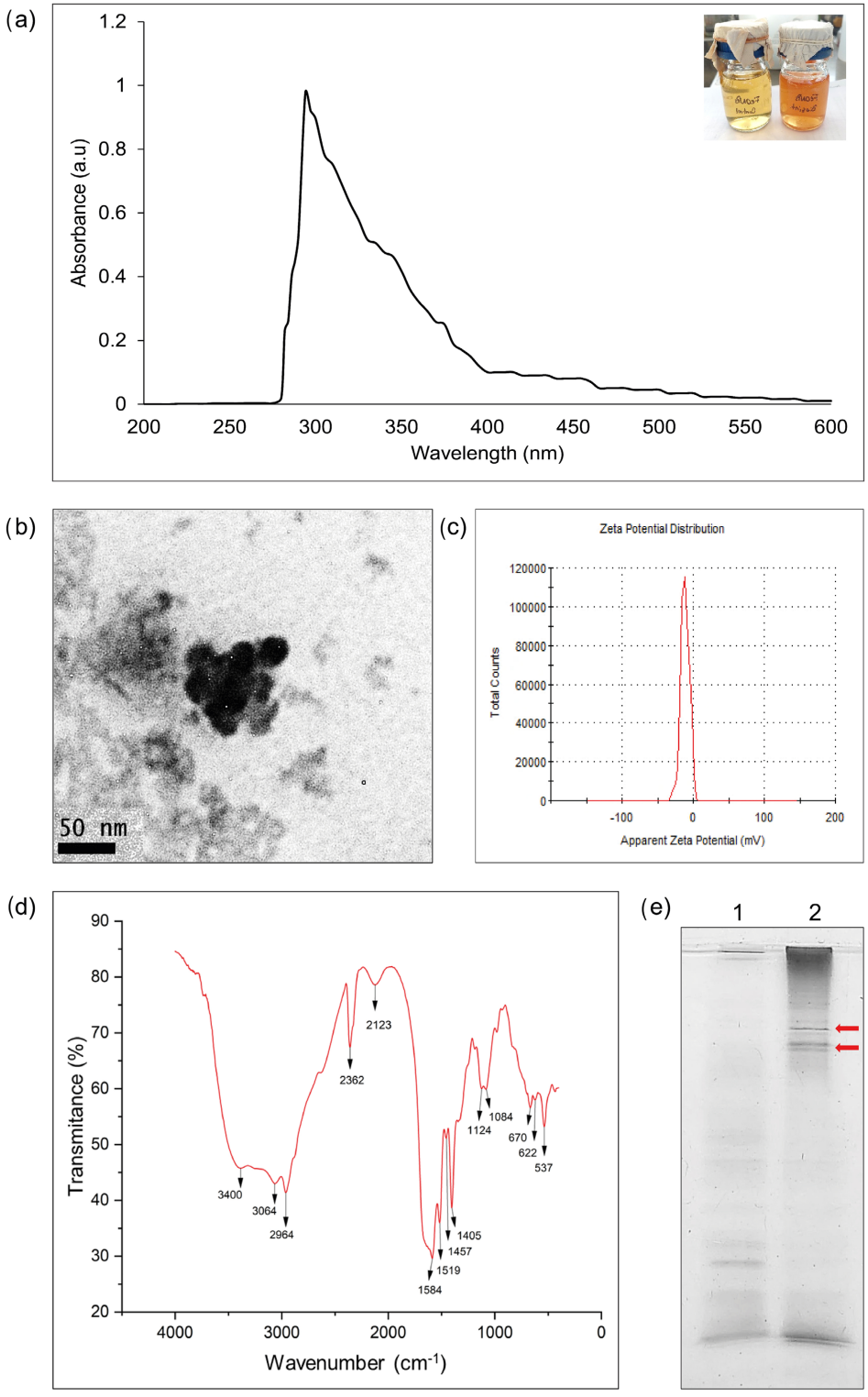

Figure S1. FeNPs biosynthesis and characterization. (a) UV–vis spectra of biosynthesized FeNPs by *E. coli* culture. The curve was recorded after 48 h incubation. Figure insert shows the culture supernatant color change from yellow to orange indicative of FeNPs presence. (b) Representative TEM image 100,000 × of the biosynthesized FeNPs. (c) Zeta potential of the biosynthesized FeNPs. (d) FT-IR spectrum of FeNPs biosynthesized by *E. coli*. (e) SDS-PAGE silver staining, line 1: supernatant; line 2: FeNPs sample. The arrows show protein bands.

of 0.46 ± 0.12. The dispersion stability of FeNPs was measured through the absolute value of zeta potential. The Z potential of FeNPs was −10.9 mV (Supplementary **Figure S1(c)**), suggesting that the FeNPs are dispersed and stabilized in the medium. EDX analysis performed by Crespo *et al.*, (2016), confirmed the presence of elemental iron and oxygen signals, suggesting that the FeNPs presented an oxide layer [1].

2.2. FT-IR Characterization and Protein Coating of FeNPs

The chemical composition of the FeNPs was characterized by FT-IR spectroscopy at room temperature (**Figure S1(d)**). Supplementary **Table S1** contains the peaks of spectra with the chemical bonds of the biosynthetic FeNPs. The peaks detected at 3400 and 3064 cm^{-1} were attributed to the O-H and N-H stretching vibrations present in polysaccharides and proteins. The peak at 2964 cm^{-1} indicates the symmetric and asymmetric stretching of CH_2 and CH_3 bonds. The peaks observed at 2362 and 2123 cm^{-1} correspond to the stretching of C=O and the C≡C and C≡N triple bonds. At 1584 cm^{-1}, the vibrations of the amine group (N-H), the carbonyl group (C=O) and the cyano group (C-N) were detected. The C=O bond stretching was also detected at 1519 cm^{-1}. The main peak at 1457 cm^{-1} could correspond to a CH_2 bond stretching or a CH_3 deformation associated with lipid proteins. The peaks detected at 1124 and 1085 cm^{-1} were mainly attributed to the vibrations of the C-O-C and P=O bonds associated with polysaccharides and nucleic acids and phospholipids, respectively. Finally, the peaks corresponding to 670, 622 and 537 cm^{-1} were attributed to the vibration of the Fe-O bond, which

Table S1. FT-IR analysis of FeNPs.

Peak (cm^{-1})	Assignment (Functional Groups)	References
3400	ν_{as} (N-H); ν (O-H)	[2]-[4]
3064	ν_{s} (N-H); ν (O-H)	[2] [5]
2964	ν_{as} (CH_x); ν_{s} (CH_x)	[3] [6]
2362	ν (C=O), ν (C≡C), ν (C≡N)	[3]
2123	ν (C≡C), ν (C≡N)	[2] [3]
1584	δ (N–H); ν (C-N); ν (C=O)	[4]-[6]
1519	ν (C=O)	[5] [7]
1457	ν (CH_2); δ_{as} (CH_3)	[5] [6] [8]
1405	ν (C=C)	[4] [6]
1124	ν_{as} (C–O–C); ν_{as} (P=O), ν (C-C)	[3] [5] [6] [8]
1084	ν_{s} (C-O-C); ν_{s} (P=O); ν (C–O)	[3] [4] [6] [8]
670	ν (Fe-O)	[9]
622	ν (Fe-O)	[5] [9]
537	ν (Fe-O)	[3] [5] [9]

confirms the production of FeNPs. In addition, the bands present in the silver-stained gel (Supplementary **Figure S1(e)**) confirm the presence of proteins that are found in FeNPs but not in the *E. coli* supernatant.

Supplementary References

[1] Crespo, K.A., Baronetti, J.L., Quinteros, M.A., Páez, P.L. and Paraje, M.G. (2016) Intra- and Extracellular Biosynthesis and Characterization of Iron Nanoparticles from Prokaryotic Microorganisms with Anticoagulant Activity. *Pharmaceutical Research*, **34**, 591-598. https://doi.org/10.1007/s11095-016-2084-0

[2] Aksu Demirezen, D., Yıldız, Y.Ş., Yılmaz, Ş. and Demirezen Yılmaz, D. (2019) Green Synthesis and Characterization of Iron Oxide Nanoparticles Using *Ficus carica* (Common Fig) Dried Fruit Extract. *Journal of Bioscience and Bioengineering*, **127**, 241-245. https://doi.org/10.1016/j.jbiosc.2018.07.024

[3] Ashrafi-Saiedlou, S., Rasouli-Sadaghiani, M., Fattahi, M. and Ghosta, Y. (2025) Biosynthesis and Characterization of Iron Oxide Nanoparticles Fabricated Using Cell-Free Supernatant of *Pseudomonas fluorescens* for Antibacterial, Antifungal, Antioxidant, and Photocatalytic Applications. *Scientific Reports*, **15**, Article No. 1018. https://doi.org/10.1038/s41598-024-84974-0

[4] Majeed, S., Danish, M., Mohamad Ibrahim, M.N., Sekeri, S.H., Ansari, M.T., Nanda, A., *et al.* (2020) Bacteria Mediated Synthesis of Iron Oxide Nanoparticles and Their Antibacterial, Antioxidant, Cytocompatibility Properties. *Journal of Cluster Science*, **32**, 1083-1094. https://doi.org/10.1007/s10876-020-01876-7

[5] Madubuonu, N., Aisida, S.O., Ali, A., Ahmad, I., Zhao, T., Botha, S., *et al.* (2019) Biosynthesis of Iron Oxide Nanoparticles via a Composite of *Psidium guavaja-Moringa oleifera* and Their Antibacterial and Photocatalytic Study. *Journal of Photochemistry and Photobiology B*: *Biology*, **199**, Article ID: 111601. https://doi.org/10.1016/j.jphotobiol.2019.111601

[6] Abu-Aqil, G., Suleiman, M., Sharaha, U., Riesenberg, K., Lapidot, I., Huleihel, M., *et al.* (2023) Fast Identification and Susceptibility Determination of *E. coli* Isolated Directly from Patients' Urine Using Infrared-Spectroscopy and Machine Learning. *Spectrochimica Acta Part A*: *Molecular and Biomolecular Spectroscopy*, **285**, Article ID: 121909. https://doi.org/10.1016/j.saa.2022.121909

[7] Chai, H., Lam, S. and Sin, J. (2019) Green Synthesis of Magnetic Fe-Doped ZnO Nanoparticles via *Hibiscus rosa*-Sinensis Leaf Extracts for Boosted Photocatalytic, Antibacterial and Antifungal Activities. *Materials Letters*, **242**, 103-106. https://doi.org/10.1016/j.matlet.2019.01.116

[8] Tang, M., McEwen, G.D., Wu, Y., Miller, C.D. and Zhou, A. (2012) Characterization and Analysis of Mycobacteria and Gram-Negative Bacteria and Co-Culture Mixtures by Raman Microspectroscopy, FTIR, and Atomic Force Microscopy. *Analytical and Bioanalytical Chemistry*, **405**, 1577-1591. https://doi.org/10.1007/s00216-012-6556-8

[9] Jubran, A.S., Al-Zamely, O.M. and Al-Ammar, M.H. (2020) A Study of Iron Oxide Nanoparticles Synthesis by Using Bacteria. *International Journal of Pharmaceutical Quality Assurance*, **11**, 88-92. https://doi.org/10.25258/ijpqa.11.1.13